BALLOON-BORNE THREE-METER TELESCOPE FOR FAR-INFRARED AND SUBMILLIMETER ASTRONOMY

Grant NAGW-509

Semiannual Status Report No. 6

For the period 1 March 1986 through 31 August 1986

Principal Investigator

Dr. Giovanni G. Fazio

December 1986

Prepared for
National Aeronautics and Space Administration
Washington, D.C. 20546

Smithsonian Institution
Astrophysical Observatory
Cambridge, Massachusetts 02138

The Smithsonian Astrophysical Observatory
is a member of the
Harvard-Smithsonian Center for Astrophysics

The NASA Technical Officer for this grant is Dr. Nancy Boggess, Code EZ-7, National Aeronautics and Space Administration, Washington, D.C. 20546

BALLOON-BORNE THREE-METER TELESCOPE FOR FAR-INFRARED AND SUBMILLIMETER ASTRONOMY

Grant NAGW-509

Semiannual Status Report No. 6

For the period 1 March 1986 through 31 August 1986

Principal Investigator

Dr. Giovanni G. Fazio

December 1986

Prepared for
National Aeronautics and Space Administration
Washington, D.C. 20546

Smithsonian Institution
Astrophysical Observatory
Cambridge, Massachusetts 02138

The Smithsonian Astrophysical Observatory
is a member of the
Harvard-Smithsonian Center for Astrophysics

The NASA Technical Officer for this grant is Dr. Nancy Boggess, Code EZ-7, National Aeronautics and Space Administration, Washington, D.C. 20546

CONTENTS

FIGURES

CONTENTS (Cont.)

TABLES

1.0 INTRODUCTION

This is the sixth Semiannual Report submitted under Grant NAGW-509 for the development of a Balloon-Borne Three-Meter Telescope for Far-Infrared and Submillimeter Astronomy. It covers the period 1 March 1986 through 31 August 1986.

The Three-Meter Balloon Borne Telescope is a joint program of the Smithsonian Astrophysical Observatory (SAO), the University of Arizona and the University of Chicago.

Effort during this reporting period focused on studying and revising the gimbal design to eliminate the alignment and limited rotation problems inherent in the flex-pivot design. A new design using ball-bearings to replace the flex-pivots has been defined and its performance analyzed. An error analysis for the entire gondola pointing system was also prepared. Arizona continued its mirror development and test program using mirror test blanks from Dornier and other sources under separate funding and will report on its effort independently. SAO, Arizona, and Chicago held telephone conferences during this period to coordinate activity and discuss technical issues.

2.0 BALL-BEARING GIMBAL DESIGN AND ANALYSIS

2.1 Candidate Design Evaluation

Two types of gimbal designs have been evaluated. The first is the baseline flex-pivot design proposed last year in the Preliminary Design Report (PDR)*; the second is the active gimbal concept proposed in the last Semiannual Report (#5, April 1986) which uses ball-bearings to support the telescope.

The advantage of the flex-pivot designs were detailed in the PDR. Further examination of the concept revealed several design weaknesses all of which relate to the limited rotation range of the flex-pivot. A long period of undisrupted tracking requires a large stiff flex-pivot which is difficult and expensive to fabricate. The flex-pivot design also requires a secondary actuation system to unwind the flex-pivots accumulated rotation due to tracking and to move the telescope through large angles when acquiring a new source. Recent experience on an SAO balloon borne spectrometer also revealed that a flex-pivot based design would require precise alignment across the telescope frame at a level difficult to maintain in the field.

The ball-bearing design provides unlimited angulation without the need for a secondary drive system. The graininess and slip-stick which they exhibit in slow-speed servos is compensated for by using a feed-forward path in the torque motor servo loop driven by bearing torque measurements.

---

* Balloon-Borne Three-Meter Telescope for Far Infrared and Submillimeter Astronomy Preliminary Design Report, Semiannual Report #4, Grant NAGW2-509, October 1985.

The torque sensor, which has an appropriate torsional spring rate, permits telescope rotation while the ball-bearings are locked by graininess or slipstick friction. While this design does have certain inherent non-linearities which the baseline design avoided, the feed forward servo incorporated in the design can compensate for them more than well enough to achieve the desired pointing accuracy and stability.

2.2 Ball-Bearing Gimbal Mechanical Design

The mechanical design is shown in Figure 2-1. A backplate acts as a pedestal on which the servo components are mounted. The torque sensor is rigidly attached to the backplate on one end and is machined on the other to mount a matched pair of angular contact bearings. These bearings provide the required rotation via a spindle which has the servo motor stator and position resolver armature mounted to it. It also provides the bolt pattern for attachment to either the telescope or X-elev frame. The backplate also has provisions for mounting the servo motor armature and position resolver stator.

The torque sensor is a commercial device which has the appropriate structural load capacity for all normal operational situations. During severe load applications (parachute deployment and crash landing for example) the torque sensor will deflect until the diameters of the servomotor mount and bearing spindle come into contact. This contact will then carry all such severe loads with a factor of safety ≥ 3 insuring that rupture and/or separation between the telescope and gondola cannot occur.

This design allows complete assembly and functional checkout of the gimbal to occur at the sub-assembly level. Two completed gimbals are then

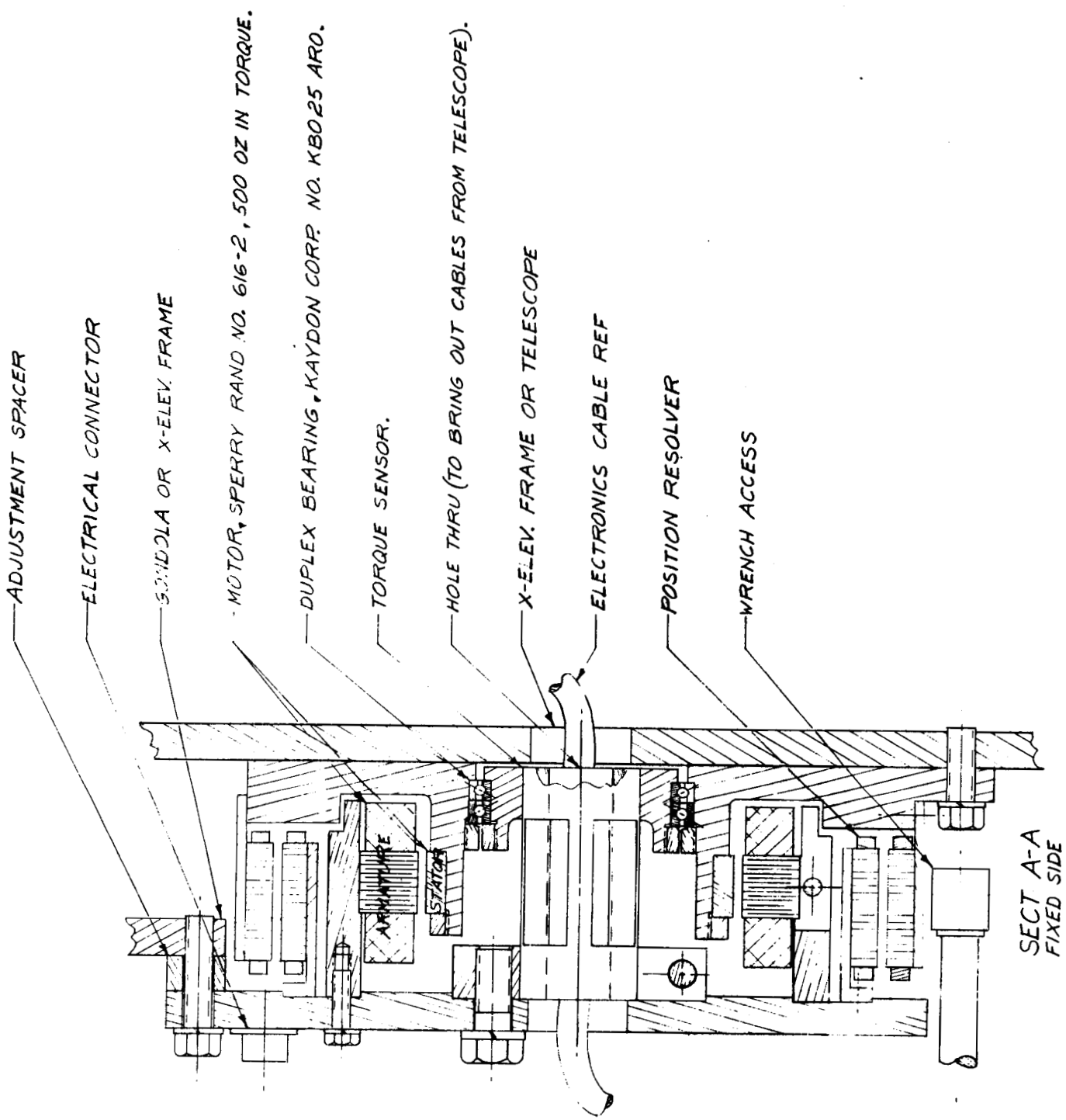

Figure 2-1. Gimbal Assembly

installed between the Telescope X-elevation frame and gondola X-elevation frame (one per side) to form the telescope elevation mount. This installation is easily accomplished by centering the telescope in the frame and attaching the gimbal assemblies to each by using the appropriate hardware. All hardware required is accessible from the outside to facilitate this attachment. The same gimbal design is also used in the cross-elevation servo.

2.3 Ball-Bearing Gimbal Servo Concept

The Servo System operates in two modes:

1) Magnetometer Mode - Celestial position acquisition controlled by the course servo loops, and

2) Inertial Mode - Inertial tracking via the fine position servos.

During initial source acquisition (Magnetometer Mode) the coarse loops in both axes are active. During inertial tracking the azimuth coarse loop acts only to dump excess momentum accumulated in the reaction wheels and to keep the telescope centered within the gimbal travel.

2.3.1 Inertial Mode (Fine Position Servo) -

2.3.1.1 Description of Fine Position Servo System -

During inertial tracking the control loop consists of four elements*:

1) The prime attitude control loop,

2) The gyro update arm,

3) The momentum management loop, and

4) The active bearing assembly.

The fine control loops in both elevation and cross-elevation take into account telescope inertia, reaction wheel behavior, gyroscope behavior and designed-in control laws. A simple proportional plus derivative controller was selected for the inertial loop. Its projected bandwidth is 2 Hz with a .7 damping ratio and it will be implemented in software. Integral feedback is not required as steady state errors are implicitly corrected within the momentum management loop. Space Telescope wheels were selected for the reaction wheels. Gyroscopes are used as the primary inertial reference and are drift corrected by a coaligned startracker. These positional updates take place every 1 to 5 seconds, too slowly to use this information directly within the fine control loops, however, more than fast enough for updating the gyros.

The reaction wheel momentum is transferred from the telescope structure to the gondola by the gimbals' brushless torque motor. The

---

* See also Section 2.4 of the PDR

reaction wheel velocity is monitored and is used to generate a proportional torque from the torque motor in the same direction. This causes the telescope to angulate. The change in position is noted by the prime inertial loop which, while compensating for this motion, causes the reaction wheel to slow down. The operation of the momentum management system is mathematically similar to integral feedback and therefore acts to correct steady state errors.

Finally, the active bearing assembly operates as a torque-free gimbal for the telescope. The gimbal consists of a ball-bearing, torque sensor, and a brushless torque motor (the same one used in the momentum management system). As the telescope rotates, the bearings generate friction torque, which is measured and compensating torques fed into the gimbal by the torque motor. This is not a closed loop system and the torque motor reaction time is important. By keeping this time as short as possible the effects of bearing "graininess" or slip-stick behavior are minimized and the chances of an interaction between the telescope attitude control loop and the active bearing are avoided. In order to successfully cancel the torque generated by the bearing the torque motor constants must be well understood. The motor will be calibrated at all orientations and conditions of expected operation. If necessary, a look-up table of torque constants will be used in demanding torque from the motor.

Each gimbal assembly cancels the torque created by its' bearing. This prevents the bearing torque from distorting the mirror cell. Which gimbal assembly to select for momentum management is still an open question. Both are equally capable of dealing with the momentum transfer, but whether to split the load equally between the gimbals assemblies or give the duty to one entirely has not yet been determined.

The cross elevation fine loop is virtually identical to the elevation fine loop, however its range of travel and interaction with the gondola and coarse loop are different. The cross elevation axis has less than ±4° of motion. The gimbal is kept centered within this range by occasional activation of the azimuth coarse loop. The cross-elevation gimbal, as it moves, changes orientation with respect to the gondola, since it is the inner gimbal. Therefore, when cross elevation momentum is dumped into the gondola it will excite a complex gondola motion which is not necessarily around an axis parallel to the cross elevation gimbal. Passive methods for damping this gondola momentum will be required.

2.3.1.2 Selected Components -

(a) Gimbal Motor

The d-c gimbal motor is a high-performance design from Sperry's Aerospace and Marine Group for use on the Space Telescope and is designated as their model 2940616-2. The motor's key features which recommend it strongly in this application are:

1) It is a brushless motor.

2) It has been specifically designed to have an extremely low ripple torque. Sperry specifies its ripple as 0.5% maximum, but states that this typically tests out to less than 0.25%. This is a percentage of the applied torque, which in our case is expected to be very low (no more than the break-free torque of the gimbal bearing, ~.1 NM).

3) Cogging torque is also designed to be very low. In this model, it

is specified as 0.4 oz-in. maximum (0.8 oz-in, peak-to-peak). The spatial frequency of the cogging torque is 48 cycles per rotor revolution (equal to the number of stator teeth).

4) The rotor-to-stator air gap is large (.120 in.) and the torque characteristics of the motor are relatively unaffected by de-centering of the rotor by as much as .030 in. This allows for sag in the torque sensors which support the full weight of the telescope in elevation, and eases the alignment requirements on the gimbal assemblies.

Note that in the final application, it may be necessary to accurately "map" the fine-scale torque variations as a function of rotation angle for each individual motor. This information will be used to correct the torque-cancelling current fed forward across the gimbal, increasing the precision of the cancellation, and therefore reducing the demands placed on the outer servo position loop.

(b) Reaction Wheels

Space telescope reaction wheels or their equivalent have been selected based on the points below:

1) Their 0.8 Nm torque capacity meets our requirements.

2) They have been thoroughly characterized during the space telescope buildup.

3) They have been selected for a number of up coming missions (AXAF and GRO, among others) thus making them readily available.

(c) Torque Sensor

The torque sensor selected is one of a class produced by Brewer Engineering, a subsidiary of Teledyne. The sensor element consists of four rectangular cross section posts machined in a cylindrical piece of metal. The cross sectional area and cylinder diameter is varied to achieved different torque sensitivities and load carrying capacities. Though Brewer Engineering provides these elements fully packaged, we would only use the bare element to reduce the gimbal's size. The specification of the package elements is given in Table 2-1 taken from a Brewer data sheet. We would use an A-05 type device.

(d) Position Encoder (Resolver)

The telescope's position with respect to the gondola must be known with sufficient accuracy to compensate for gimbal motor torque anomalies. Also, the elevation servo loop requires this information when operating in Magnetometer Mode in order to generate an appropriate error signal. Both requirements call for a readout device with absolute position accuracy of ±5 arcminutes.

Many of the same considerations involved in the choice of the gimbal torque motor enter here also. The sensor must not introduce any significant disturbing torque across the gimbal, it should mount on a hollow shaft (to allow cable pass-through) and its performance must be relatively insensitive to decentering.

One device which meets all these requirements is a brushless resolver. In particular Sperry has supplied on special order position resolvers with extremely wide radial air gaps, accommodating radial translation up to

Type A Torque Sensors

Capacities
10, 20, 50, 100, 200, 500, 1,000, 2,000
5,000, 12,000 and 30,000 in-lbs
(larger capacities available)

Performance
Output at rated torque (R.T.) ..... 1.5 mv/V
Calibration accuracy ..... 0.25% R.T., CW or CCW
Nonlinearity
10-50 in-lbs ..... 0.10% R.T.
all others ..... 0.05% R.T.
Repeatability ..... 0.05% R.T.
Hysteresis
10-50 in-lbs ..... 0.15% R.T.
all others ..... 0.05% R.T.

Temperature
Temperature range, safe ..... -50 to 140° F
compensated .... 0 to 140° F
Temp. effect on rated torque ..... 0.005% Reading per ° F
Temp. effect on zero balance ..... 0.0025% R.T. per ° F

Electrical
Excitation, recommended ..... 12 V, AC or DC
maximum ..... 25V, AC or DC
Zero balance @ 72 ± 3° F ..... 2.5% R. T.
Terminal resistance, input ..... 350 ± 1.5 ohms
output ..... 350 ± 3 ohms

Termination MS3102A-18-8S-A105 connector with mating 15-ft. cable assembly

Insulation resistance
bridge to ground ..... 2,000 megohms
shield to ground ..... 1,000 megohms

Overload Ratings
Safe 120%
Electrical failure 300%

Options:
Consult factory for minor dimensional modification and available RPM sensors

Dynamic Characteristics
Type A

TORQUE PICKUP TYPE	CAPACITY (IN-LBS)	MAX. SPEED (RPM)	WR^2 ($LB\text{-}IN^2$)	FLEXURAL NATURAL FREQUENCY (RPM)	TORSIONAL STIFFNESS (IN-LB/RADIAN)	WEIGHT (LBS)	FIGURE
A-001	10	3,600	.634	15,500	300	3	1
A-002	20	3,600	.636	17,500	900	3	1
A-005	50	3,600	.643	23,000	2,300	3	1
A-01	100	7,000	1.26	46,600	14,800	5.5	2
A-02	200	7,000	1.26	46,600	14,800	5.5	2
A-05	500	7,000	1.32	81,800	79,700	6	2
A-1	1,000	7,000	1.56	86,600	72,600	6	2
A-2	2,000	5,000	2.69	29,200	99,300	17	3
A-5	5,000	5,000	2.78	31,800	238,000	17.5	3
A-12	12,000	5,000	22.6	37,400	905,000	39	4
A-30	30,000	5,000	23.5	41,600	1,680,000	42	4

NOTE: The tabulated data pertains to the torque pickup only and does not include the effects of couplings or other rotating masses that would be part of a dynamic system.

Table 2-1. Torque Sensor Specifications

±.200 inch, and having an accuracy of ±1 minute of arc. A modification of one of their standard space-qualified designs has been tentatively adopted by us for the present application, and is shown in the gimbal mechanical assembly (Figure 2-1).

2.3.1.3 Full System Model -

A nonlinear system block diagram is shown in Figure 2-2. This is similar to Figure 2.4-3 on page 53 of the PDR. The notable differences are the inclusion of the ball-bearing in the flex-pivot/ball-bearing block, the ball-bearing deflection, its accumulation, and the explicit representation of the gimbal motor's time constant. The nature of the ball-bearing deflection, which acts to reduce the quantity and thus the torque across the ball-bearing and sensor is not clearly definable. The deflection must be assumed to be nonlinear and therefore beyond the capabilities of our present computer model. Fortunately, however, linear modelling does provide useful results.

(a) The Linear Model Configuration

Telescope angulation for most fine-pointing operations is absorbed by the torque sensor. The torque sensor acts as a flexure since for small angles the ball-bearing will be locked by friction. When the stored torque in the flexure reaches the bearing release friction the bearing will rotate. While there are many scenarios for the behavior of the bearing at the time of release, the anticipated worst case is a snap that will recenter the torque sensor (i.e., to zero torque). This can be seen by the following scenario: If the bearing were to relieve slowly the torque sensor would follow the relaxation and demand less torque from the gimbal

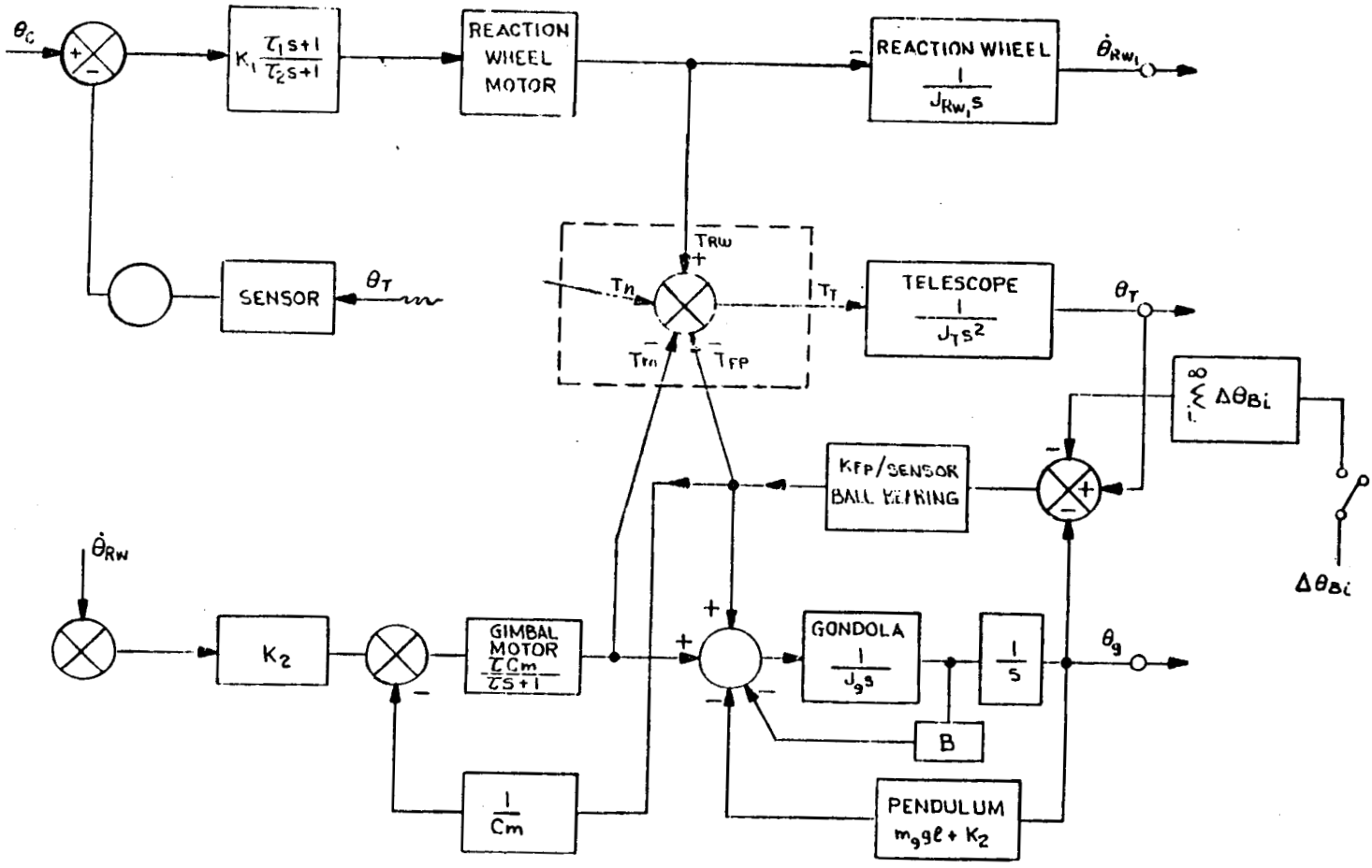

Figure 2-2. Nonlinear System Block Diagram

motor. Ideally this would be transparent to the telescope as the gimbal motor would always track the bearing torque. However, if the bearing snapped back to the torque sensor's center point, the torque sensor and motor would not have time to follow and the net torque on the telescope and gondola would be that applied by the motor. The motor torque would decay to zero as the sensor reading and motor driver electronics overcome the motor time constant. Under these conditions, the telescope would be subjected to a torque pulse approximately .2-.5 Nm in height and about 10 ms (four times the motor time constant) in duration.

A linear model can be constructed from these assumptions. It yields a model of the pointing system from which worst case performance can be judged. In this model the telescope is suspended on a torque sensor, has two controlled torque sources, the reaction wheel and the gimbal, and is subjected to occasional noise pulses of 5×10^{-3} Nms. The noise pulses model the bearing snap. The results of this analysis are given below (Section 2.3.1.4). This linear analysis obviously does not predict limit cycle or other characteristic nonlinear behavior.

(b) Nonlinear Model

In a nonlinear model the torque sensor would be compared to the break-free frictional torque of the bearing. When these torques were equal the nonlinear representation of the bearing motion would be triggered. The boxed-in node in the block diagram representation of the system depicted in Figure 2-2 is where this non-linear behaviour is modeled. The torque felt by the telescope would be given by the time-dependent equation:

$$T(t) = \Delta \theta_{Bi}(t) \bullet K_{FP/S}$$

for as long as the ball-bearing deflected. The exact nature of the model nonlinearity (as opposed to the true system nonlinearity) would be twofold:

1) The comparator operation between the sensor torque and the break-free frictional torque when it results in the switch (i.e., the bearing breaks away and its symmetric operation to freeze the bearing motion), and

2) The nature of the function $\Delta\ \theta_{Bi}\ (t)$.

However, the rest of the model and the equations are the same as the linear representation. This nonlinearity only presents itself when the telescope has moved sufficiently to cause the flexure or sensor to develop a torque equal to that of the bearing break-free torque. The required angle for break-free torque is about 1° and depends on the sensor spring constant and the bearing properties.

The telescope's prime operation is tracking stars, which rotate at a maximum rate of 15°/hr. In operation, the bearing nonlinearity will be excited on the order of once every four minutes, which is infrequent in light of the 2 Hz control bandwidth.

The linear model does not show any limit cycle behavior which might result from the bearing's stiction, however, we can determine if a limit cycle may result by looking at the system response to the bearing noise pulse. If the telescope motion is large it may excite a further bearing release (not shown by the linear model) and thus enter a limit cycle; If it is small no limit cycling occurs. The linear simulation indicates that in fact the telescope motion is small enough to avoid exciting limit cycle behavior.

(c) Development of System Equations

For the development of the linear equations please refer to Appendix A in which Appendix B of the PDR is reproduced. Referring to page A-14 we see that in the new system model the figure of the torque summing junction is still valid and the same as that shown in Figure 2-2 in the dashed enclosure. In fact equations (1)+(2) of the appendix are still valid, as far as they go. The model for the proposed design only changes from the baseline in its control law for the gimbal motor. Thus equation (5) on page A-16 of the appendix will become:

$$T_{Gm} = K_2\dot{\theta}_{RW} - T_{FP} \qquad (1)$$

where: T_{FP} = the torque-sensor torque

(note a typo lists $\dot{\theta}_{RW}$ as $\ddot{\theta}_{RW}$ in the original text.)

$$\text{Now } T_{FP} = K_{FP}\ (\theta_g - \theta_T)\,. \qquad (2)$$

By adding equation (1) here to equation (1) of the appendix (page A-14) the result is removal of the dependency on K_{FK} and thus cancellation of the effect of the flex-pivot, or spring constant of the torque sensor.

Therefore, if we follow this through to page A-17, equations 8-13 remain valid if we set K_{FP} to zero.

The ball-bearing shows up as an impulse under T_N, noise torque, to which we must determine the system response.

2.3.1.4 System Response -

System behavior was simulated using the computer program "TF" written at Stanford University. This program provided a Bode plot (see Figure 2-3) and an impulse response (Figure 2-4) for the modelled system. The impulse assumed for the sake of the analyses was $5x10^{-3}$ Nms as mentioned above, applied at T=0, it resulted in a maximum predicted excursion of the telescope from its commanded position of .025 arcsec. At such a small angle the system behavior begins to be quantized by the digital-to-analog converters and cannot be considered strictly linear, so the response shown in Figure 2-4 may not be a realistic prediction of system response. However, we do see that the "snapping" of the ball-bearing has little effect on the telescope pointing.

The rest of the model behavior is nearly identical to the system described in the PDR. The new gimbal model predicts that the telescope is completely isolated from the gondola. This is different from the earlier system model in which the telescope was explicitly coupled to the gondola behavior by the flex-pivot. In practice, the gondola will excite some telescope motion through the nonlinearities in the gimbal.

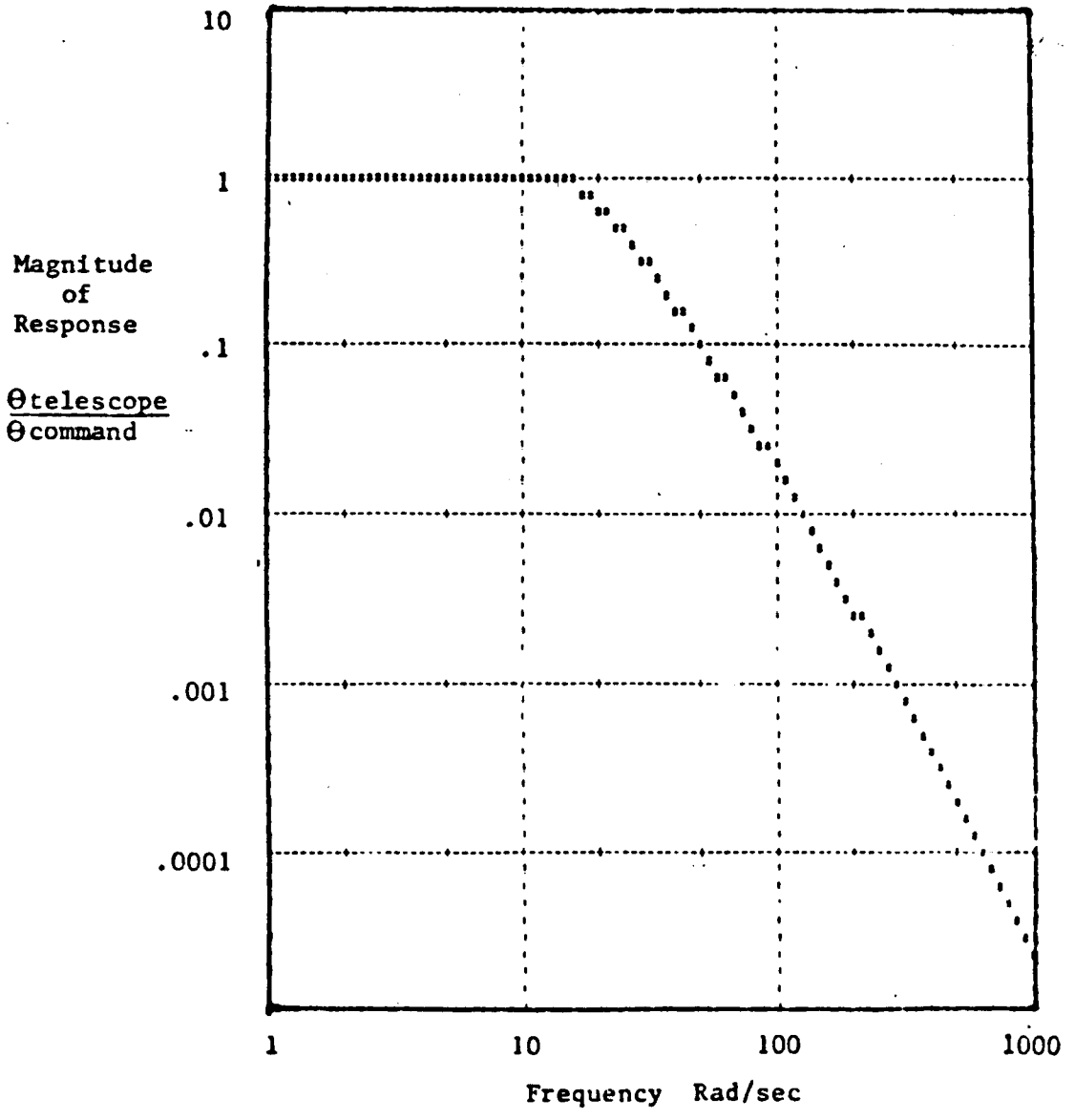

Figure 2-3. Fine-Pointing Control System Response to a Sinusoidal Command Signal

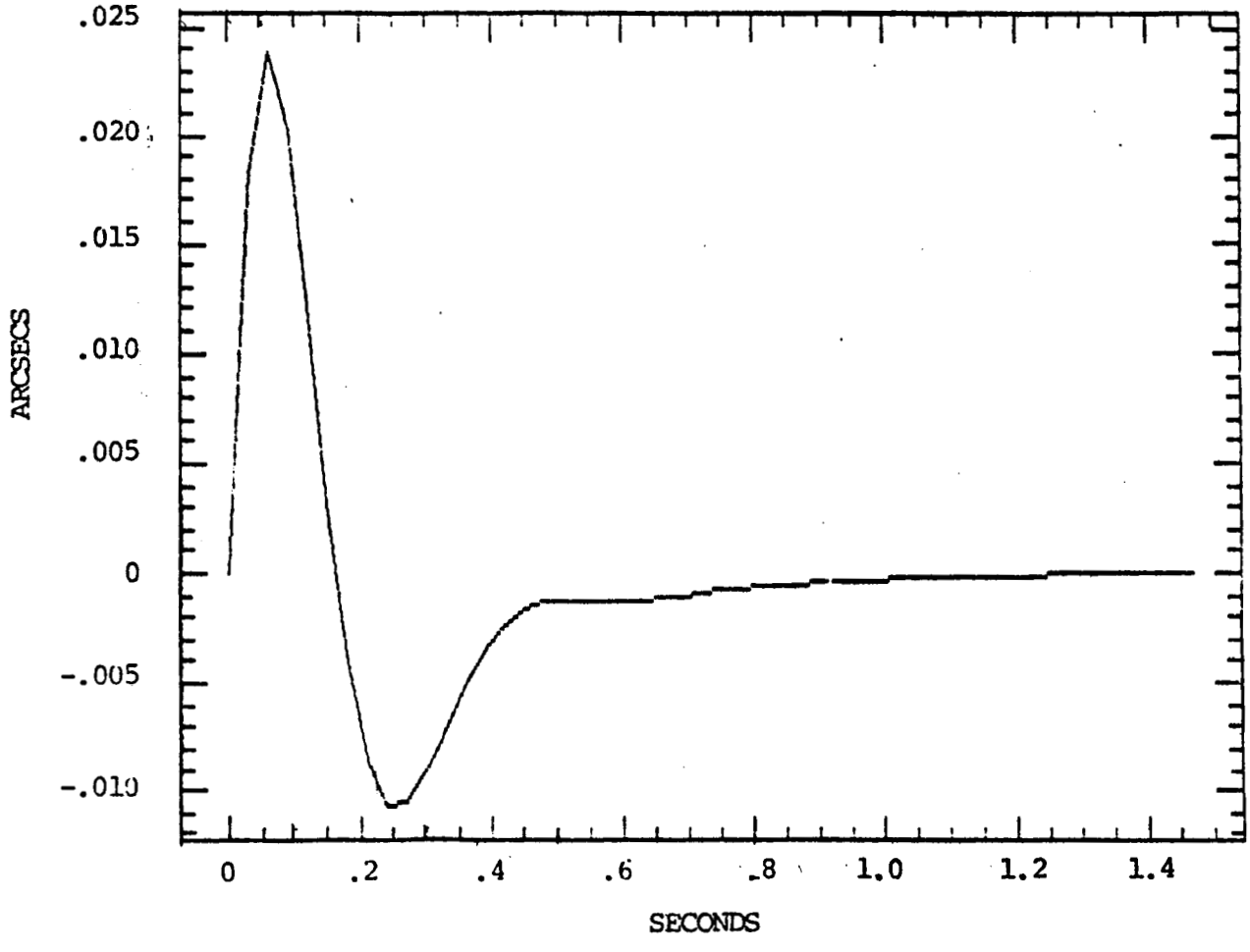

Figure 2-4. Telescope Point Response to a 5×10^{-3} Nms Torque Pulse

2.3.2 Azimuth Servo (Coarse Loop) -

The Azimuth Servo is the outermost control loop. It is a coarse pointing loop, which contains the cross-elevation, or fine loop within it. The functions of this outer loop are threefold:

1) In Magnetometer Mode, the Azimuth Servo is used for the initial acquisition of a targeted celestial object, and points the gondola to within ±30 arcminutes of the commanded location. This is close enough to allow recognition of the star field in the aspect TV camera. Azimuth reference in this mode is the earth's magnetic field, as sensed by a Schonstedt flux-gate magnetometer. The inner gimbal is driven to its center position and locked while the target is being acquired.

2) In Inertial Tracking Mode, the error input which drives the Azimuth Servo is switched from the magnetometer to the inner gimbal position sensor and the inner gimbal is unlocked, allowing the cross-elevation fine servo to become active. The Azimuth Servo then maintains coarse orientation of the gondola so that the target object remains well within the limited range of the cross-elevation gimbal. Our present intention is to include a threshold, or dead-banding, feature so that the outer loop becomes active only when the inner gimbal moves away from its center position more than some minimum angle. This will reduce the amount of activity in the Azimuth servo, and result in fewer disturbance torques for the pointing control to cope with.

3) The coarse Azimuth servo also serves as a means of dissipating

momentum built up in the cross-elevation reaction wheel. When this momentum is dumped (by torquing the cross-elevation gimbal motor) a component of it, proportional to the cosine of the elevation angle, is coupled into the gondola azimuth axis. The azimuth reaction wheel responds by taking on a velocity and this energy is removed by the azimuth loop twisting against the suspension lines.

A full block diagram of the combined Cross-elevation and Azimuth servos, showing their areas of interaction is shown in Figure 2-5.

A more complete explanation of the overall system concept, and descriptions of the subsystem elements, is contained in the PDR, Section 2.4.4, "Pointing System Control Laws and Predicted Performance".

2.3.3 Summary -

The ball-bearing gimbal design presented in this report will satisfy the pointing requirements of the telescope without the initial alignment, secondary drive system, and limited angulation inherent in the earlier design.

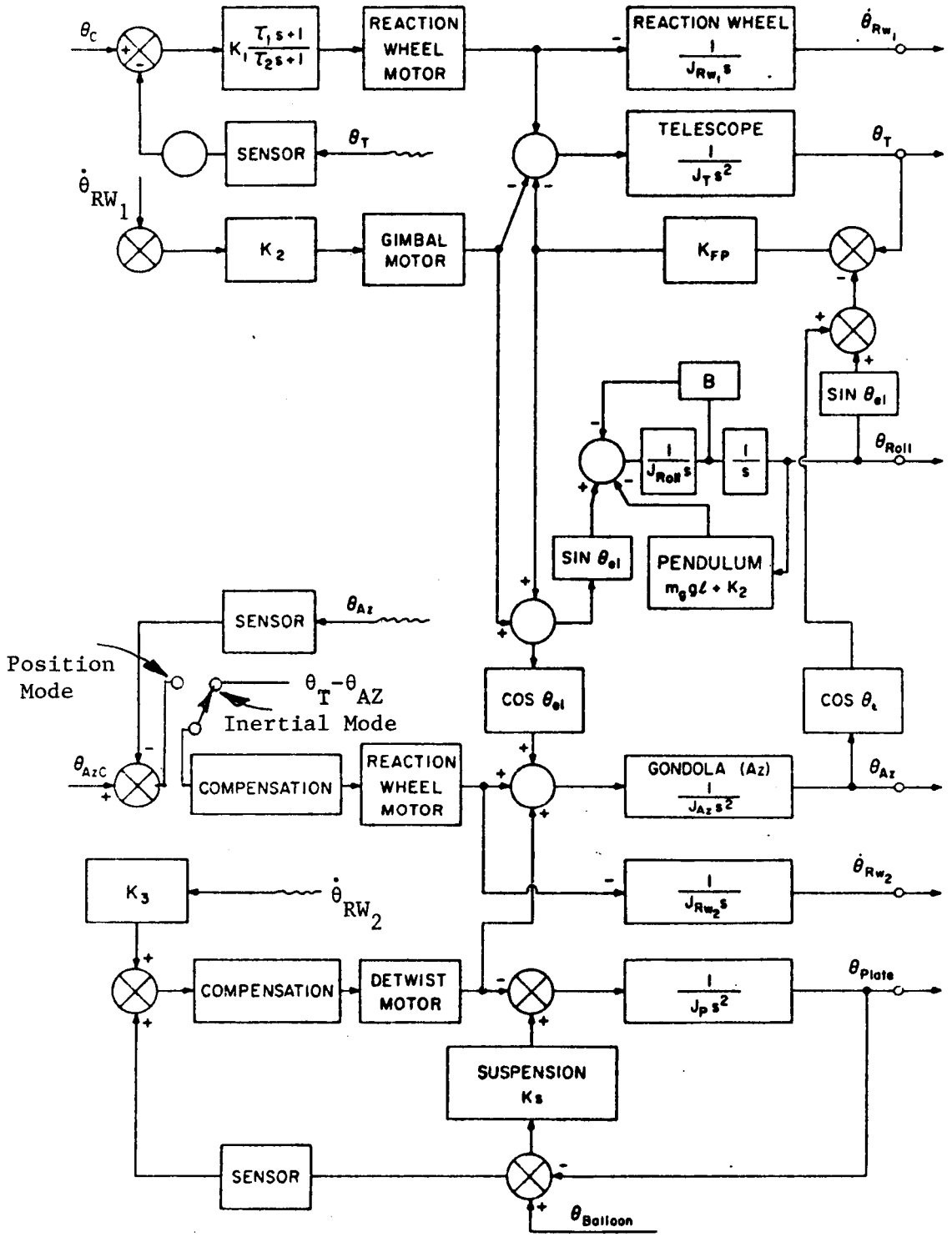

Figure 2-5. Block Diagram of Azimuth and Cross-Elevation Servos

3.0 SYSTEM ERROR ANALYSIS

An error analysis has been performed for three different star tracker configurations:

1) Co-aligned but outside the focal plane of the telescope;

2) Beamsplitter feed at the focal plane;

3) Direct IR focal plane measurement by a high resolution instrument.

These results are based on error magnitudes that have been taken from the PDR or if unavailable these, assigned on the basis of best engineering judgment. The values of 1.0, 0.61 and 0.30 arcsecs RMS were calculated for image position precisions for the three star tracker configurations respectively.

3.1 Configurations

3.1.1 Co-Aligned Star Tracker -

The co-aligned star tracker is the present baseline design as described in the PDR.

3.1.2 Beamsplitter Feed - Focal Plane Star Tracker -

The beamsplitter feed star tracker consists of a star tracker like the one proposed for the baseline, viewing a target or guide star image folded from the main telescope image. This arrangement has several advantages over the baseline:

1. The star tracker can compensate for secondary motions which would otherwise result in image motion at the focal plane;

2. The structural separation between the tracker and the focal plane is smaller and thus the tracker is less likely to move relative to the focal plane;

3. The star tracker can compensate for image displacement resulting from relative motion between the primary mirror and its housing.

The disadvantages of this arrangement are:

1. The mirrors must be of optical quality in the visible wavelengths to yield an image usable to the star tracker;

2. There is a beamsplitter between the secondary and the infrared experiment which results in light loss to both the star tracker and instrument.

3. The beamsplitter star tracker leg of the star tracker optical path is still separate from what is being stabilized (i.e. the focal plane image), thus motions in that leg or in the focal plane would result in an image error.

3.1.3 Instrument Star Tracker -

The third arrangement examined was one using a high resolution camera in the focal plane to yield a tracking signal. This arrangement has all the advantages of the previous one with none of its listed disadvantages. Furthermore the system does not have to be boresighted as the star tracker and the telescope line-of-sight (LOS) are identical.

3.2 Error Sources

The possible error sources are split into two categories: Fixed and Operational. The fixed errors are those which either cannot be removed during boresighting or do not vary with time (e.g. those resulting from imprecise knowledge). The operational errors are those which occur during flight.

3.2.1 Fixed Errors -

The fixed errors are the base irreducible system errors . In the two boresighted arrangements these are the boresighting accuracies, in the other, the only fixed error is measurement error in determining the center of the focal plane.

The error sources inherent in the boresighted designs are:

1. Control system pointing performance
2. Star Camera boresight uncertainty
3. Focal Plane CCD boresight uncertainty

4. Unremovable secondary decenter precision, and

5. Focal plane boresight uncertainty

The control system and star camera values were taken from the PDR, the others are best estimates. The focal plane boresight accuracy was assumed to be equal to that of the star camera. The unremovable decenter tolerance requires that the secondary mirror be placeable to ±.0008 cm, which can be considered a specification for that system. The focal plane boresight uncertainty requires that the focal plane geometry be known to ±.002 cm; neither of these requirements are difficult to achieve.

3.2.2 Operational Errors -

The operational errors are:

1. Gravitationally induced truss deflection,
2. Star tracker misalignment,
3. Star tracker centroid accuracy,
4. Control system noise,
5. Truss thermal deflection,
6. Secondary decenter,
7. Secondary misalignment, and
8. Mirror/housing relative motion.

These all effect the coaligned star tracker arrangement; 2, 3, and 4 effect the beamsplitter system and only 3 and 4 effect the instrument star tracker.

The gravitationally induced truss deflection results from the fact that the viewing and the boresighting elevation angles are different and the gravity gradient across the truss therefore changes at the sidereal rate. The star tracker misalignment is taken from the PDR for the co-aligned arrangement and assigned for the beamsplitter case. It should be noted that a co-alignment of .6 arcseconds between the star tracker and the telescope is achievable, but is considered a difficult specification. Star tracker centroid and control system errors come directly from the PDR. The thermal deflection of the truss, the secondary misalignment and misplacement, and the mirror/housing relative motions each cause focal plane image motion through two coupled mechanisms. 1) secondary decenter, and 2) secondary misalignment. The mirror/housing motion does not cause true secondary motion but it can be treated as if it does.

All calculations assume that the system is boresighted prior to each observation. The contribution of image blur to the image position error was reviewed, found to be minor and thus not included. The two errors resulting from each source are first added together algebraically before root-square-summing these values with errors resulting from other uncorrelated sources. The precisions assigned to the secondary mechanisms and the primary mirror to housing motion are estimates. We conclude that it will not be possible to achieve one arcsecond total pointing error without the use of a focal plane guider.

The various R.S.S. of the errors are presented in the lower part of Table 2-2 along with the total fixed and operational error.

Table 3-1. System Error Performance for Three Star Tracker Configurations

Fixed Error	Focal Plane Tracking		Parallax Star Camera Co-aligned
	Using Resolving instrument	Using Beam Splitter to feed star camera	
Control System		.2	.2
Star Camera		.2	.2
Focal Plane CCD		.2*	.2*
Unremovable decenter		.1*	.1*
Imprecise knowledge of focal plane	.1*	.1*	.1*
Total Fixed Error - RSS	.1	.37	.37
Operational Error			
Mirror/housing relative motion			1.0*
Truss deflection field errors (one hour after boresighting)			0.11
Star tracker misalignment		.4*	.6
Star tracker centroid	.2	.2	.2
Control system	.2	.2	.2
Truss thermal deflection (1°C gradient)			0.2
Secondary misplacement			.1*
Secondary misalignment			.1*
Total operational error	.28	.49	1.23
Total error - RSS	.30	.61	1.28

*Estimate or assigned value

Note: all numbers are arcsec RMS of apparent image motion at the focal plane.

3.3 Determination Of The Relationship Between Secondary Misplacement And Image Motion

The alignment tolerance shown in Table 2.2-2 of the PDR were used as the basis for establishing the relationship between secondary decenter and misalignment, and image motion. The values in Table 2.2-2 of the PDR are given as allowable errors in secondary placement for a 1 arcsec apparent image displacement in the field. As such these values are not, strictly speaking, ratios between secondary motion and apparent image angular displacement. However, for this error analysis they have been used that way. In defense of this approach all the image motions resulting from secondary displacement are near and less than 1 arcsec thus treating the relationship as linear is not going to be far wrong.

An example of how these calculations are done, in the case of the effect of mirror/housing relative motion on image stability, is given below.

First the primary mirror relative motion is translated into apparent secondary decenter and misalignment.

Secondary Decenter:

$$\Delta_{Apparent} = \phi_M \bullet \ell_T \qquad (1)$$

where: $\Delta_{Apparent}$ is the apparent displacement of the secondary -(cm)

ϕ_M is the actual mirror motion -(radian)

ℓ_T is the interoptic spacing -(cm)

Secondary Misalignment:

$$\phi_{Apparent} = \phi_M \text{ (radian)} \qquad (2)$$

From Table 2.2-2 the secondary decenter tolerance for a 1 arcsec image stability is -.0022 cm while the misalignment tolerance is .06647 arcmin for the same image stability. The resulting image motion from a given ϕ_M is then found as follows:

Secondary Decenter:

$$\alpha FE_D = \frac{-\Delta_{Apparent}}{.0022} \qquad (3)$$

or from eg. (1)

$$\alpha FE_D = \frac{-\phi_M \ell_T}{.0022} \qquad (4)$$

where: αFE_D is the apparent image motion or field effect due to displacement.

Secondary Misalignment:

$$\alpha FE_M = \frac{\phi_M (57 \bullet 60)}{.06647} \qquad (5)$$

where: $(57 \bullet 60)$ is to convert from Radians to arcmins.

The total image motion is given by:

$$\alpha FE_T = \alpha FE_D + \alpha FE_M \qquad (6)$$

and

$$\alpha FE_T = \frac{-\phi_M \ell_T}{0.0022} + \frac{\phi_M (57 \bullet 60)}{0.06647} \qquad (7)$$

$$\alpha FE_T = 51{,}452\phi_M - 454.44\phi_M \ell_T \qquad (8)$$

4.0 RESEARCH PLANNED FOR NEXT REPORTING PERIOD

Engineering analysis and design under this grant is complete. Effort during the next reporting period will follow research presently underway in producing lightweight mirrors and we will continue our discussions with foreign groups or possible collaborators on this project.

APPENDIX A

Pointing Control System Servomechanism Analysis

Glossary of Symbols

Θ_c Angular command (desired pointing) of mirror assembly with respect to inertial space

Θ_m Angular response (actual pointing) of mirror assembly with respect to inertial space

ε_m Angular pointing error of mirror assembly

J_W Moment of inertia of momentum wheel

τ_{TM} Torque developed by momentum wheel torque motor

J_m Moment of inertia of mirror assembly

τ_{ext} External torque applied to mirror assembly

k Spring rate of flex-pivot suspension of mirror assembly [torque units per radian]

T_M Torque developed by ancillary torque motor

Θ_H Angular position of Horseshoe gimbal with respect to local vertical

J_H Moment of inertia of Horseshoe gimbal

ω_H Frequency of angular vibration of Horseshoe gimbal [rad/sec]

S Laplace operator

$\dot{\Theta}_W$ Angular velocity of momentum wheel with respect to inertial space

K' Ancillary torque motor conversion gain [torque units per rad/sec]

AK_τ Amplifier-Torque motor constant [torque units per radian]

T_1 Lead time constant of lead/lag network

T_2 Lag time constant of lead/lag network

$\tau_{applied}$ Total systemic torque applied to the pendulous Horseshoe gimbal (reaction of ancillary torque motor and flex-pivot)

τ_ν Torque Noise (bearing torque noise, motor cogging, etc.)

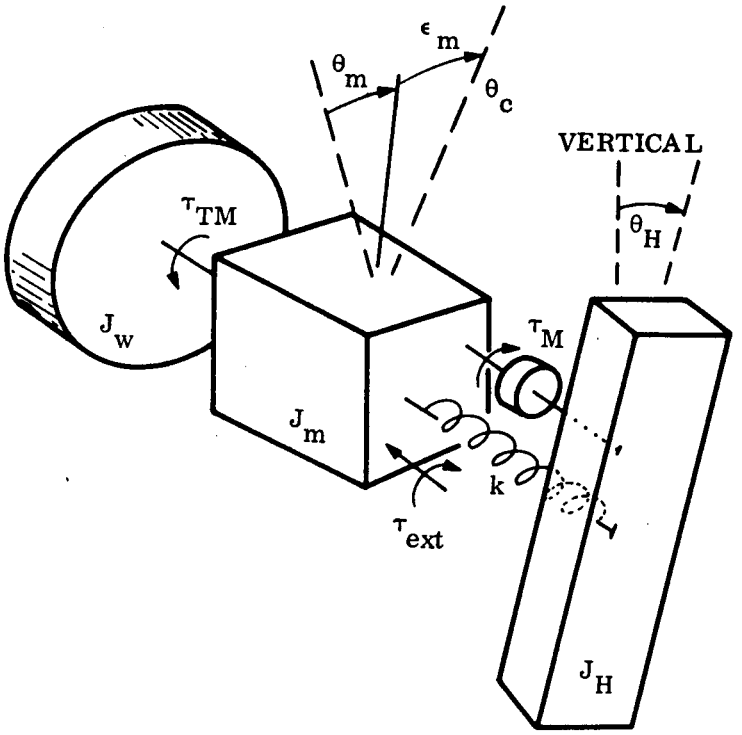

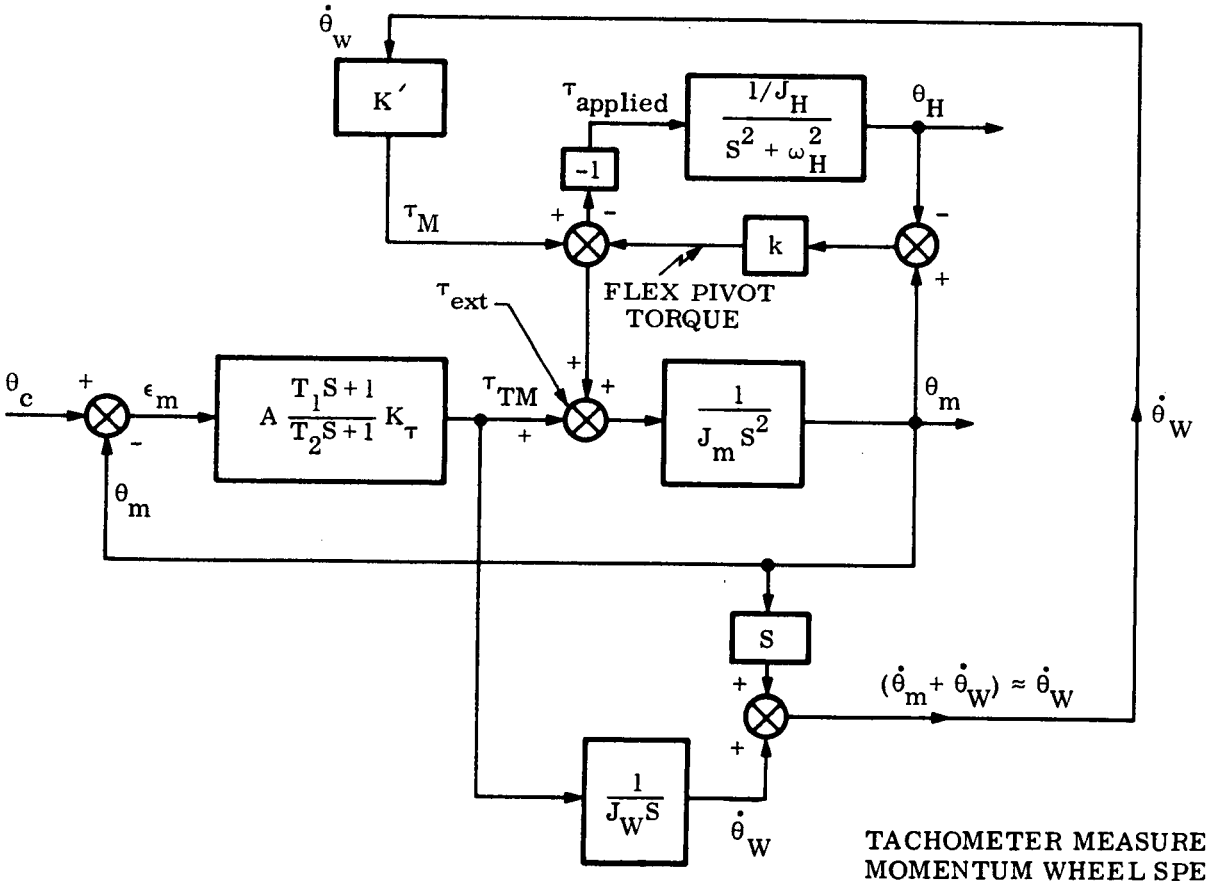

TACHOMETER MEASURE OF MOMENTUM WHEEL SPEED

System Dynamics Equation is:

$$\begin{bmatrix} \left[J_m S^2 + \frac{T_1 S+1}{T_2 S+1} AK_\tau \left(1 + \frac{K'}{J_W S}\right) + k\right] & -k \\ -\left[k + \frac{T_1 S+1}{T_2 S+1} AK_\tau \frac{K'}{J_W S}\right] & \left[\left(S^2+\omega_H^2\right)J_H+k\right] \end{bmatrix} \begin{Bmatrix} \Theta_m \\ \Theta_H \end{Bmatrix} =$$

$$\begin{Bmatrix} \frac{T_1 S+1}{T_2 S+1} AK_\tau \left(1+\frac{K'}{J_W S}\right)\Theta_c + \tau_{ext} \\ -\frac{T_1 S+1}{T_2 S+1} AK_\tau \frac{K'}{J_W S}\Theta_c \end{Bmatrix}$$

Determinant is:

$$\Delta(S) = \frac{1}{S}\left\{ J_m J_H S^5 + \left(J_m J_H \omega_H^2 + J_m k + J_H k\right) S^3 + \frac{T_1 S+1}{T_2 S+1} AK_\tau \left[\left(S^2+\omega_H^2\right)\left(J_H S + \frac{K' J_H}{J_W}\right)+kS\right] + \omega_H^2 J_H k S \right\}$$

which can be recast in form of:

$$\Delta(S) = \frac{1}{S(T_2 S+1)} \left\{K_6 S^6 + K_5 S^5 + K_4 S^4 + K_3 S^3 + K_2 S^2 + K_1 S + K_0\right\}$$

Stable!

Full System Response to Pointing Command

$$\Theta_m = \frac{\begin{bmatrix} \frac{T_1 S+1}{T_2 S+1} AK_\tau \left(1+\frac{K'}{J_W S}\right)\Theta_c + \tau_{ext} & -k \\ -\frac{T_1 S+1}{T_2 S+1} AK_\tau \frac{K'}{J_W S}\Theta_c & \left[(S^2+\omega_H^2)J_H+k\right] \end{bmatrix}}{\Delta(S)}$$

or

$$\Theta_m = \frac{1}{\Delta(S)} \left\{ \left[(S^2+\omega_H^2) J_H \frac{T_1 S+1}{T_2 S+1} AK_\tau \left(1+\frac{K'}{J_W S}\right) + k\frac{T_1 S+1}{T_2 S+1} AK_\tau \right]\Theta_c + \left[\left(S^2+\omega_H^2\right)J_H+k \right] \tau_{ext} \right\}$$

Final value of mirror pointing is:

$$\Theta_m\Big|_{s.s.} = \lim_{S\to o} S\Theta_m(S) = \lim_{S\to o} \frac{1}{\Delta(o)} \left\{ \left[\omega_H^2 J_H AK_\tau \left(1+\frac{K'}{J_W S}\right) + kAK_\tau \right]\Theta_c + \left[\omega_H^2 J_H+k\right]\tau_{ext} \right\}$$

or

$$\Theta_m\Big|_{s.s.} = \lim_{S\to o} \frac{1}{\omega_H^2 \frac{K'J_H}{J_W}AK_\tau} \left\{ \left[\omega_H^2 J_H AK_\tau \left(S + \frac{K'}{J_W} \right) + kAK_\tau S \right] \Theta_c + \left[\omega_H^2 J_H + k \right] S\, \tau_{ext} \right\}$$

$$= \frac{1}{\omega_H^2 \frac{K'J_H}{J_W}AK_\tau} \left\{ \omega_H^2 \frac{K'J_H}{J_W}AK_\tau \right\} \Theta_c$$

$$= \Theta_c$$

with zero final error even with torsional flex-pivots, external torque, and disturbing horseshoe-motion coupling.

FREQUENCY DOMAIN ERROR ANALYSIS

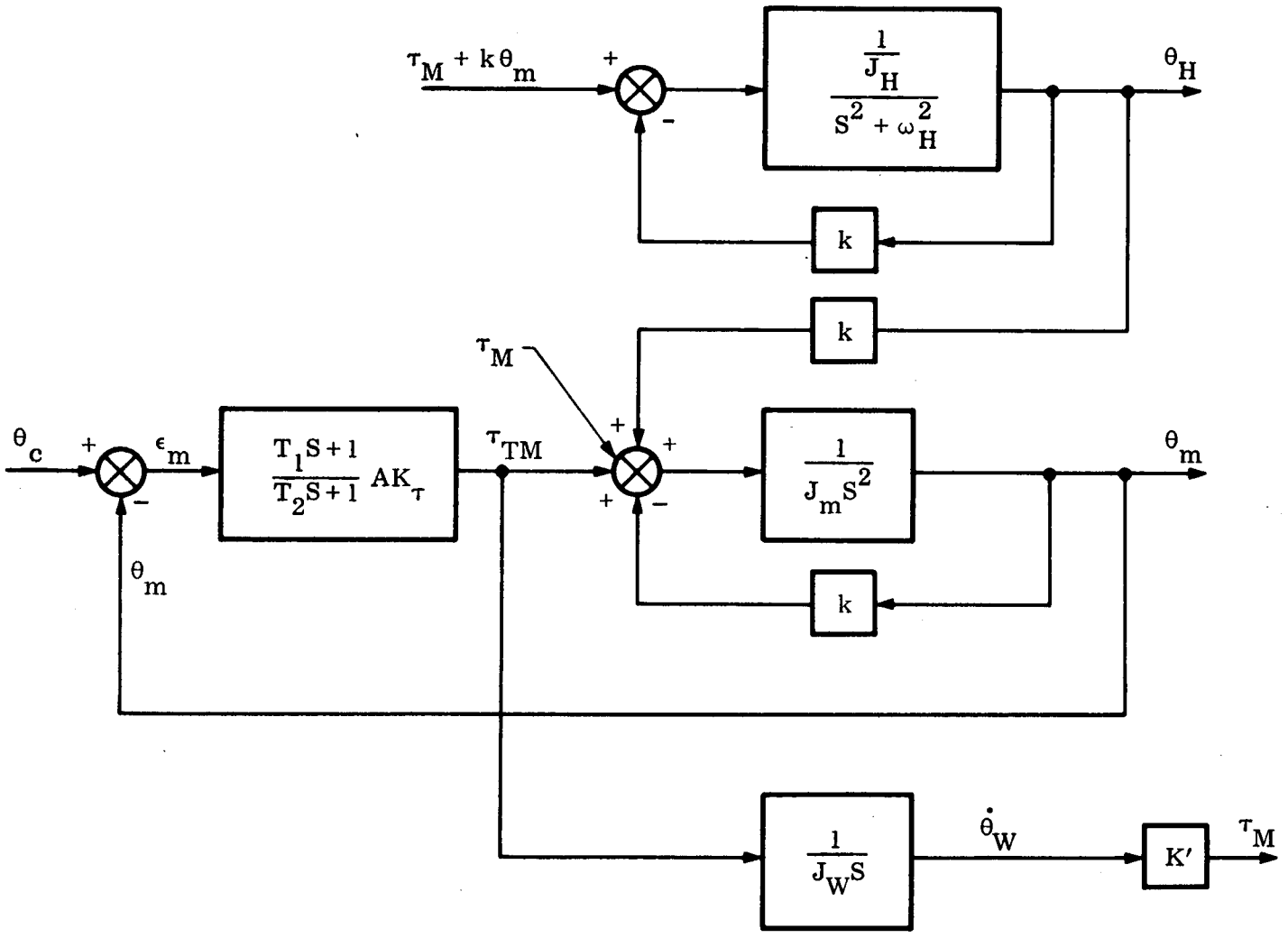

Mirror spectral sensitivity to Horseshoe Gimbal motion is given by:

$$\frac{\Theta_m}{\Theta_H} = \frac{\left(k\,\frac{J_W}{J_m}\right)\left(T_2S+1\right)S}{K_4S^4 + K_3S^3 + K_2S^2 + K_1S + K_0}$$

where

$$K_4 = T_2J_W$$

$$K_3 = J_W$$

$$K_2 = \left(\frac{J_W}{J_M}\,kT_2 + \frac{J_W}{J_m}\,AK_\tau T_1\right)$$

$$K_1 = \left(\frac{J_W}{J_m}\,k + \frac{AK_\tau K'}{J_m}\,T_1 + \frac{J_W}{J_m}\,AK_\tau\right)$$

$$K_0 = \frac{AK_\tau K'}{J_m}$$

Note: •Zero at origin reduces steady-state sensitivity to zero.

•Sensitivity at "horseshoe" gimbal frequency is given by above equation

FREQUENCY DOMAIN SKETCH OF SPECTRAL SENSITIVITY

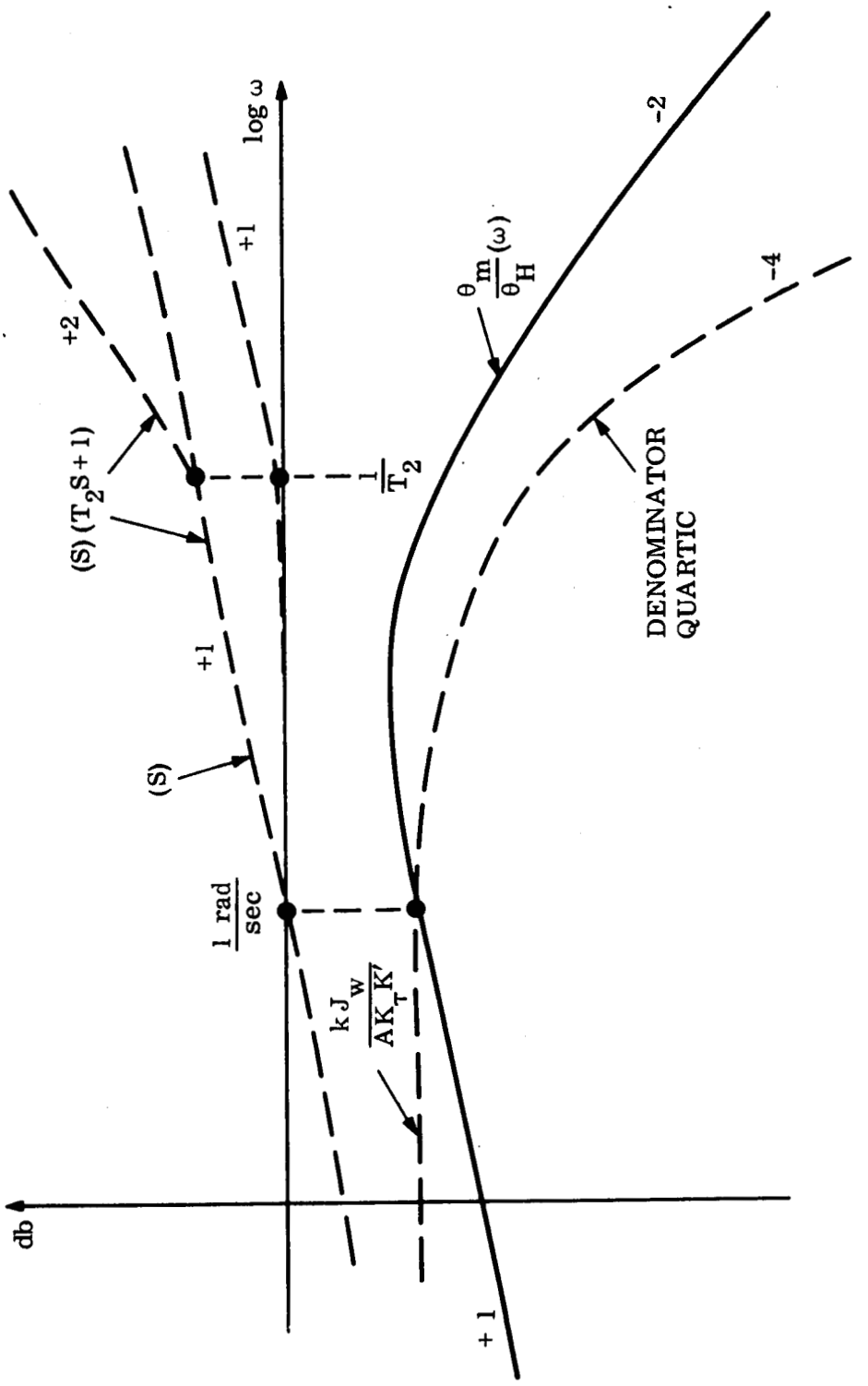

Because "horseshoe" gimbal characteristic frequency, ω_H, is very low, the low frequency asymptote of spectral sensitivity expression may be used:

$$\boxed{\frac{\Theta_m}{\Theta_H} \approx \frac{k\ J_w\ \omega}{A\ K_\tau\ K'}}$$

where $\omega = \sqrt{\omega_H^2 + \frac{k}{J_H}}$, rad/sec

k = flex-pivot constant, [torque units per radian]

J_W = momentum wheel moment of inertia [torque units per radian/sec^2]

AK_τ = amplifier torque motor constant [torque units per radian]

K' = ancillary torque motor conversion gain [torque units per rad/sec.]

J_H = horseshoe moment of inertia [torque units per rad/sec^2]

System Spectral Sensitivity to Torque Noise

$$\frac{\Theta_m}{\tau_\nu}(S) = \frac{1}{\Delta(S)} \left\{ (S^2+\omega_H^2)J_H+k \right\}$$

or

$$\frac{\Theta_m}{\tau_\nu}(S) = \frac{S[T_2S+1][S^2+\omega_H^2+\frac{k}{J_H}]J_H}{K_6S^6+K_5S^5+K_4S^4+K_3S^3+K_2S^2+K_1S+K_0}$$

where:

$$K_6 = J_m J_H T_2$$

$$K_5 = J_m J_H$$

$$K_4 = [(J_m J_H \omega_H^2+J_m k+J_H k)T_2+AK_\tau J_H T_1]$$

$$K_3 = \left[J_m J_H \omega_H^2+J_m k+J_H k+AK_\tau J_H+AK_\tau T_1 \frac{K'J_H}{J_w} \right]$$

$$K_2 = \left[AK_\tau \frac{K'J_H}{J_W} + AK_\tau(\omega_H^2 J_H+k)T_1+\omega_H^2 J_H k T_2 \right]$$

$$K_1 = \left[AK_\tau(\omega_H^2 J_H+k)+AK_\tau \omega_H^2 T_1 \frac{K'J_H}{J_w} + \omega_H^2 J_H k \right]$$

$$K_0 = AK_\tau \omega_H^2 \frac{K'J_H}{J_w}$$

SPECTRAL TORQUE-NOISE SENSITIVITY

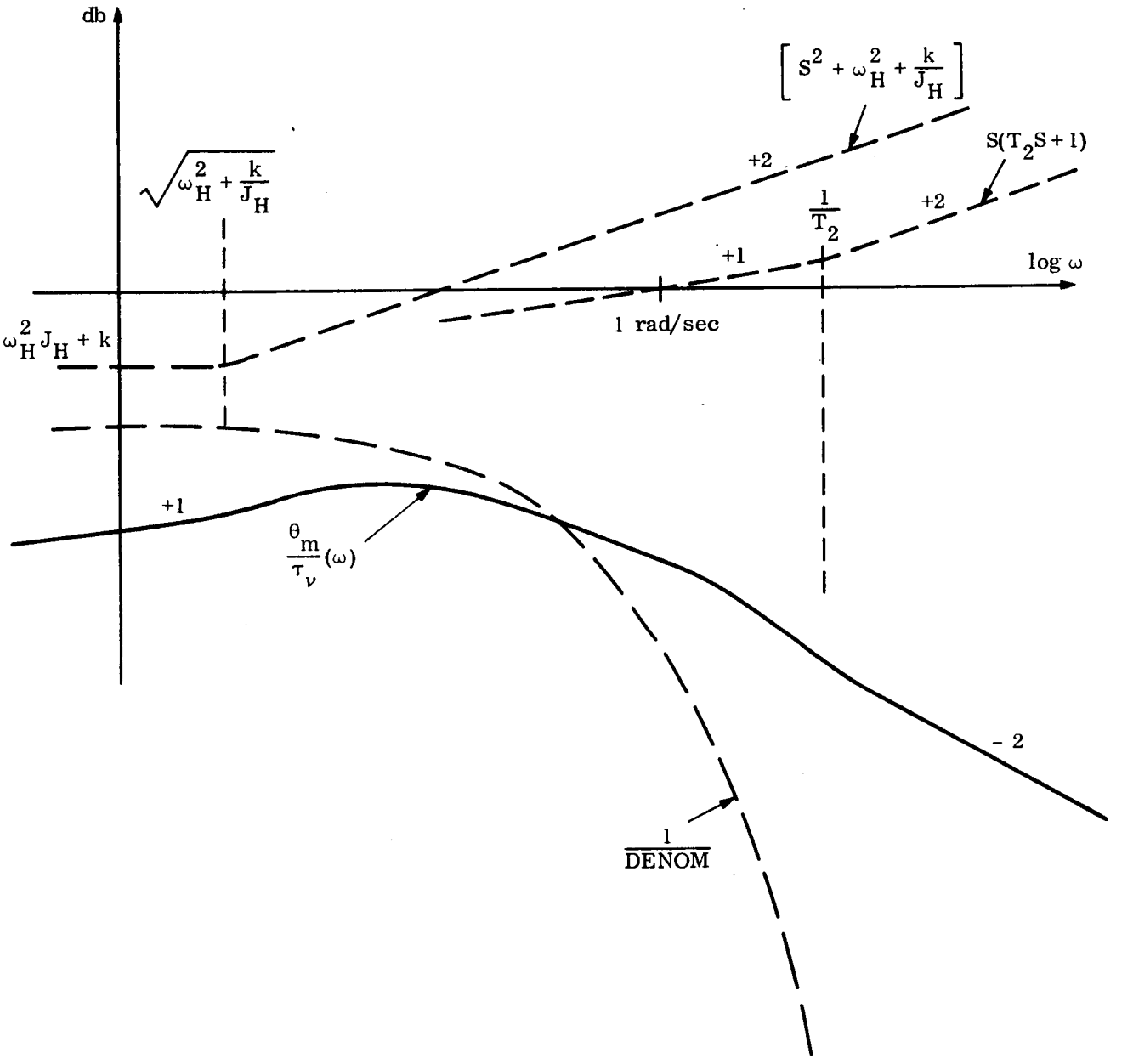

The <u>low frequency</u> asymptote may be approximated by:

$$\frac{\Theta_m}{\tau_\nu} \approx \frac{\left(\omega_H^2+\frac{k}{J_H}\right)J_H}{AK_\tau \omega_H^2 \frac{K'J_H}{J_W}} \omega_\nu$$

(low freq.)

$$\approx \frac{\left(\omega_H^2 + \frac{k}{J_H}\right)J_W}{AK_\tau \omega_H^2 K'} \omega_\nu$$

$$\approx \frac{J_W}{AK_\tau K'} \omega_\nu$$

<u>where</u> ω_ν is the circular frequency of the torque-noise in rad/sec.

Generic Control

The controlled system can be written as:

$$\ddot{X}_T = -K_{FP}/J_T \, X_T + T_c/J_T + \frac{X_c \, K_{FC}}{J_T} \tag{1}$$

where X_T is the angle being controlled

K_{FP} is a spring constant

J_T is an inertia

T_c is the control torque

X_c is the command input

If we select a simple proportional plus rate controller we have:

$$T_c = -K_g \, (\dot{X}_T \, \tau + X_T) \tag{2}$$

where: τ is the zero location of the controller

K_g is the control gain

Combining (2) and (1) and rewriting we get:

$$\ddot{X}_T + \frac{K_g \tau}{J_T} \dot{X}_T + \frac{(K_{FP} + K_g)}{J_T} X_T = \frac{K_{FP}}{J_T} X_c \tag{3}$$

The generic equation for a 2nd order system like this is:

$$\ddot{X} + 2\zeta\omega_n \dot{X} + \omega^2_n X = \omega_n^2 X_c \tag{4}$$

where: ζ is the damping ratio

ω_n is the natural frequancy

If we select ω_n, ζ we can match coefficients between (4) & (3):

$$\frac{K_g + K_{fp}}{J_T} = \omega^2_{n_o} \tag{5}$$

$$\frac{K_g \, \tau}{J_T} = 2\zeta_o \omega_{n_o} \tag{6}$$

In this way we solve for K_g and τ and get our control.

The individual loops are then combined into a system of equations and solved. Some adjustments are made for the ignored coupling.

Elevation Axis Equation.

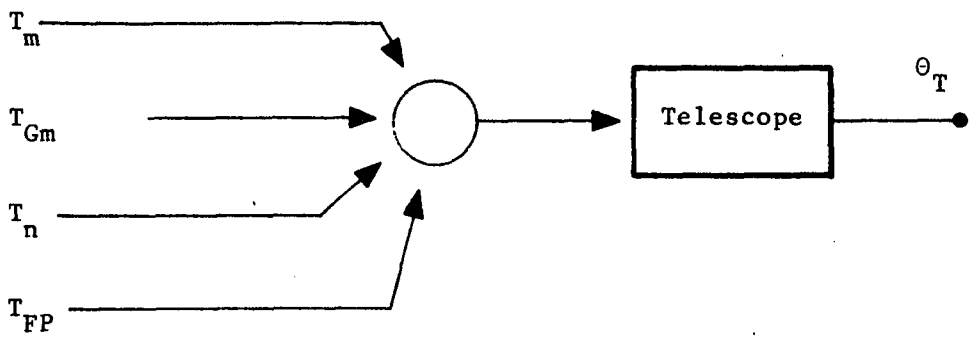

The equation of motion of the telescope is:

$$J_T\ddot{\Theta}_T = K_{FP}(\Theta_g - \Theta_T) + T_{Gm} + T_m + T_n \qquad (1)$$

where: J_T is the telescope inertia

Θ_T is the telescope angular position

K_{FP} is the flex-pivot sprint constant

Θ_g is the gondola's angular position

T_{Gm} is the gimbal motor torque

T_m is the reaction wheel motor

T_n is noise torque

The equation of motion for the gondola is

$$J_g\ddot{\Theta}_g = K_{Fp}(\Theta_T - \Theta_g) - T_{Gm} - \omega_p{}^2 J_g \Theta_g \qquad (2)$$

where: ω_p is the compound pendulum natural frequency.

Elevation Axis Equation (continued):

Equation of motion of the Reaction Wheel is:

$$J_{r\omega}\,\ddot{\Theta}_{R\omega} = -T_m \tag{3}$$

The control law states:

$$T_m = k_1 \frac{(\tau_1 S+1)}{(\tau_2 S+1)} \tag{4}$$

&

$$T_{Gm} = K_2 \ddot{\Theta}_{R\omega} \tag{5}$$

If we put these equations into state space form as the following:

$$\left.\begin{aligned} X_1 &= \Theta_T \\ X_2 &= \dot{\Theta}_T \\ X_3 &= \Theta_g \\ X_4 &= \dot{\Theta}_g \\ X_5 &= \dot{\Theta}_K \\ X_6 &= \Theta_1 \end{aligned}\right\} \tag{6}$$

where: Θ_1 is used to define a state existing in the control law or:

$$T_m = K_1\,\Theta_1 \tag{7}$$

Elevation Axis Equations:

Eqs. (1), (2), (3) & (4) with eqs. (6) can be put into 6 first order differential equations:

$$\dot{X}_1 = X_2 \tag{8}$$

$$\dot{X}_2 = \frac{1}{J_T}\left[-K_{Fp}\, X_1 + K_{Fp}\, X_3 - K_2\, X_5 + K_1\, X_6 + T_n\right] \tag{9}$$

$$\dot{X}_3 = X_4 \tag{10}$$

$$\dot{X}_4 = \frac{1}{J_g}\left[K_{Fp}\, X_1 - X_3\,(K_{Fp} + \omega_p{}^2\, J_g) + K_2\, X_5\right] \tag{11}$$

$$\dot{X}_5 = -\frac{K_1}{J_{F\omega}}\, X_6 \tag{12}$$

$$\dot{X}_6 = \frac{1}{\tau_2}\left[-X_1 - \tau_2\, X_2 - X_6 + X_6\right] \tag{13}$$

Where: X_6 is the commanded signal for the telescope. These equations can be placed in matrix form as

$$\underline{\dot{X}} = [A]\underline{X} + [B]\underline{u} \tag{14}$$

where: [A] is the matrix of coefficients of the x_i's

$$\underline{u} = \begin{bmatrix} x_c \\ T_n \end{bmatrix}$$

$$[B] = \begin{bmatrix} 0 & 0 \\ 0 & \frac{1}{J_T} \\ 0 & 0 \\ 0 & 0 \\ 0 & 0 \\ \frac{1}{\tau_2} & 0 \end{bmatrix}$$

In this form the system was run through a program called "TF" (Transfer Function) written at Stanford University to generate system responses.